



PERGAMON

PII: S1359-6454(99)00019-1

*Acta mater.* Vol. 47, No. 5, pp. 1575–1586, 1999  
© 1999 Acta Metallurgica Inc  
Published by Elsevier Science Ltd. All rights reserved  
Printed in Great Britain  
1359-6454/99 \$20.00 + 0.00

## MODELLING OF ELASTIC CONSTANTS OF PLASMA SPRAY DEPOSITS WITH ELLIPSOID-SHAPED VOIDS

SANG-HA LEIGH and CHRISTOPHER C. BERNDT†

Department of Materials Science and Engineering, State University of New York at Stony Brook, Stony Brook, NY 11794-2275, U.S.A.

(Received 24 September 1998, accepted 4 January 1999)

**Abstract**—The five independent elastic constants of plasma spray deposits were calculated from constitutive equations and microstructural information (void aspect ratios and porosity) was gained from stereological analysis. The voids within the deposit were assumed to be ellipsoidal in shape. The structure of the deposit was considered to be transversely isotropic with respect to the spray direction, which requires five independent elastic constants of a stiffness tensor. Solid mechanics models containing ellipsoid-shaped voids were applied to obtain the five independent elastic constants of the deposits. The calculated elastic constants were compared to the experimentally determined values. © 1999 Acta Metallurgica Inc. Published by Elsevier Science Ltd. All rights reserved

### 1. INTRODUCTION

The distinct material properties of thermal spray deposits, compared to those produced by other techniques, arise from the unique material processing technique, including rapid solidification and particle impact. However, owing to the complexity and variability of the deposit formation process and a number of variables which influence the processing conditions, the formation mechanism and the microstructure of thermal spray deposits are not fully understood. Therefore, the origin of the unique material properties of thermal spray deposits is not clearly revealed.

Among several mechanical properties, elastic properties such as Young's modulus, shear modulus, bulk modulus and Poisson's ratio play a pivotal role because a wide range of mechanical properties are related to them. Thermal spray deposits are often assumed to have the same Young's moduli as bulk materials of the same chemical composition and phase. However, Young's moduli of thermal spray deposits, due to their microstructure and inhomogeneity, are known to be much lower than the comparable bulk materials. The Young's modulus values of thermal spray deposits are closely related to the microstructure, which is influenced by a number of factors such as spray method, spray condition and post-treatment. Thermal spray deposits exhibit highly anisotropic behavior that originates from the lamellar structure [1–3]. Thus, it is necessary to consider the measurement directions when determining the

Young's modulus of thermal spray deposits, or when referencing existing data in the literature.

Elastic constants of solid materials are fundamental and important material properties. Elastic constants include Young's modulus, shear modulus, bulk modulus and Poisson's ratio which are directly related to interatomic bonding. Effective elastic constants are of particular interest when dealing with porous (or cracked) materials and composites, since these microstructural factors are incorporated into experimentally estimated elastic constants.

Numerous experimental and theoretical studies have been carried out on the effective elastic constants of porous materials. Since porosity is an important issue with regard to the elastic behavior of a material, numerous experimental works have correlated porosity and the effective elastic constants [4–10]. A significant amount of theoretical work has also calculated the effective elastic constants of porous materials and composites [11–19].

Thermal spray deposits are considered to be transversely isotropic with respect to spray direction. It can be shown that five independent components of the stiffness tensor are required to completely describe the transversely isotropic case [20].

The microstructure studies of thermal spray deposits have been mostly carried out in a qualitative fashion. Extensive quantitative microstructural information is required to better understand and explain the mechanical properties of thermal spray deposits. Stereology, which describes three-dimensional information using two-dimensional sections, has been applied to quantitatively investigate the microstructural features of thermal spray deposits. Stereology enables the generation of strict micro-

†To whom all correspondence should be addressed

structural information that is not available directly from the cross-sections that most researchers and engineers study.

Several approaches lead to a quantitative analysis of a metallographic microstructure, such as the morphometry, the quantitative metallography, the stereometric metallography and the stereology. Various kinds of objects with different shapes are encountered in material structures (i.e. grains, particles, impurities, inclusions, pores and cracks) and are often assumed as certain geometrical shapes such as spheres, ellipsoids, cubo-spheres and cubes to determine the size and/or size distribution by means of stereology. In thermal spray deposits, flattened particles (i.e. splats) or voids (i.e. pores and cracks) can be approximated to spheroids [21, 22]; i.e. ellipsoids of revolution [23]. There are two ellipsoidal morphologies, prolate and oblate shapes, which are generated by the rotation of an ellipse around its major axis and minor axis, respectively. In this paper, void shapes are considered as an oblate ellipsoid

For this paper, water-stabilized plasma-sprayed  $\text{Al}_2\text{O}_3$ -13 wt%  $\text{TiO}_2$  (AT13) free-standing forms were produced and Young's modulus values were measured using four-point bend, indentation and flexural vibration tests. The void size and shape were determined from stereology, which were used to theoretically calculate the five independent elastic constants of the AT13 deposit based on a model developed by Zhao *et al.* [17]. It was found that the Young's modulus values determined from the theoretical model are comparable to the experimental results.

## 2. EFFECTIVE ELASTIC CONSTANTS OF TRANSVERSELY ISOTROPIC POROUS MATERIALS

The theoretical analysis of effective elastic constants for transversely isotropic porous materials is presented. A set of simple, explicit constitutive equations for the effective elastic constants of transversely isotropic porous materials developed by Tandon and Weng [24, 25] and Zhao *et al.* [17] is presented in this section. The shape of the pores is modeled by an ellipsoid. Two different transversely isotropic cases are presented, namely unidirectionally and two-dimensional randomly isotropic models. For each model two special cases were considered depending on the shape of the ellipsoids, i.e. penny-shaped pores and circular cracks. In this paper, equations for ellipsoidal pores are presented. For equations of special cases, refer to the original literature [17].

### 2.1. Theoretical treatment

Consider a composite with transverse isotropy subjected to a boundary traction that gives rise to a uniform stress  $\mathbf{s}$ . Also consider a reference material which has the same properties as the matrix

and which is subjected to the same boundary condition. The strain in the reference material is then uniform and related to the stress by

$$\bar{\sigma}_{ij} = C_{ijkl}^0 \bar{\epsilon}_{kl}^0 \quad (1)$$

where  $C_{ijkl}^0$  is the stiffness tensor of the matrix and  $\bar{\epsilon}_{kl}^0$  is the strain in the reference material. The strain in the composite is also related to the applied stress as

$$\bar{\sigma}_{ij} = C_{ijkl}^1 \bar{\epsilon}_{kl}. \quad (2)$$

The average stress and strain in the matrix are different from the reference material due to the inclusions. These deviations are designated as  $\mathbf{s}$ , and  $\tilde{\epsilon}_{kl}$ , and related to each other as

$$\tilde{\sigma}_{ij} = C_{ijkl}^0 \tilde{\epsilon}_{kl}. \quad (3)$$

Under a stress  $\bar{\sigma}_{ij}$ , the average stress in the matrix is given by  $\bar{\sigma}_{ij} + \tilde{\sigma}_{ij}$  and the average strain by  $\bar{\epsilon}_{kl}^0 + \tilde{\epsilon}_{kl}$ . Based on Mori-Tanaka's mean field theory [14], the average stress of the matrix is given by

$$\sigma_{ij}^{(0)} = \bar{\sigma}_{ij} + \tilde{\sigma}_{ij} = C_{ijkl}^0 (\bar{\epsilon}_{kl}^0 + \tilde{\epsilon}_{kl}). \quad (4)$$

The average stress and strain of the inclusions further differ from those of the matrix by a "perturbed" value  $\sigma_{ij}^{\text{pt}}$  and  $\epsilon_{kl}^*$ , respectively. Considering Eshelby's equivalence principle the average stress of the inclusion is given by

$$\begin{aligned} \sigma_{ij}^{(1)} &= \bar{\sigma}_{ij} + \tilde{\sigma}_{ij} + \sigma_{ij}^{\text{pt}} = C_{ijkl}^1 (\bar{\epsilon}_{kl}^0 + \tilde{\epsilon}_{kl} + \epsilon_{kl}^{\text{pt}}) \\ &= C_{ijkl}^0 (\bar{\epsilon}_{kl}^0 + \tilde{\epsilon}_{kl} + \epsilon_{kl}^{\text{pt}} - \epsilon_{kl}^*) \end{aligned} \quad (5)$$

where  $\epsilon_{kl}^*$  is the equivalent transformation strain introduced into the regions occupied by the inclusions. Thus, the stiffness tensor  $C_{ijkl}^1$  can be replaced by  $C_{ijkl}^0$  to provide an identical  $\sigma^{(1)}$ . The perturbed strain is related to the equivalent transformation strain by Eshelby's tensor [20], i.e.

$$\epsilon_{kl}^{\text{pt}} = S_{klmn} \epsilon_{mn}^*. \quad (6)$$

From equations (4) and (5), the perturbed stress is expressed as

$$\sigma_{ij}^{\text{pt}} = C_{ijkl}^0 (\epsilon_{kl}^{\text{pt}} - \epsilon_{kl}^*). \quad (7)$$

The balance of the stress requires that  $\bar{\sigma}_{ij} = c_1 \sigma_{ij}^{(1)} + c_0 \sigma_{ij}^{(0)}$ , which gives rise to

$$\tilde{\sigma}_{ij} = -c_1 \sigma_{ij}^{\text{pt}} \text{ or } \tilde{\epsilon}_{kl} = -c_1 (\epsilon_{kl}^{\text{pt}} - \epsilon_{kl}^*). \quad (8)$$

The strain of the composite  $\bar{\epsilon}_{kl}$  is given by the volume average of strains over its matrix and inclusions, i.e.

$$\bar{\epsilon}_{kl} = \bar{\epsilon}_{kl}^0 + c_1 \epsilon_{kl}^*. \quad (9)$$

The equivalent transformation tensor is obtained from equation (5) in terms of  $\bar{\epsilon}_{kl}^0$ , i.e.

$$(C^1_{ijkl} - C^0_{ijkl})[\epsilon^0_{kl} + (1 - c_1)S_{klmn}\epsilon^*_{mn} + c_1\epsilon^*_{kl}] + C^0_{ijkl}\epsilon^*_{kl} = 0. \tag{10}$$

Consequently, the effective elastic constants of the composite can be derived from equations (1), (2) and (9).

2.2. Unidirectionally aligned ellipsoidal pores

Based on the theory described in Section 2.1, the five independent elastic constants for unidirectionally isotropic porous materials can be developed [17–25]. Considering a case of symmetry with regard to axis 1 (refer to Fig. 1 for orientation notation), the five independent elastic constants are given by:

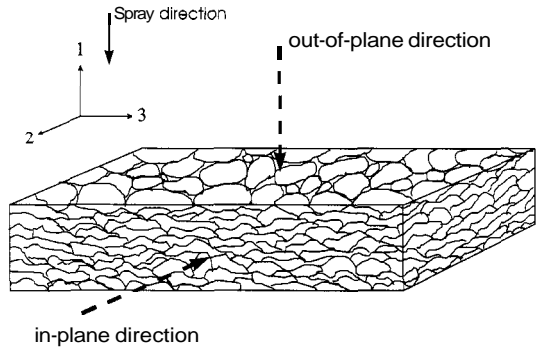


Fig. 1. Notation of direction for transversely isotropic thermal spray deposits.

$$\frac{E_{11}}{E_0} = \frac{1}{1 + c_1(A_1 + 2\nu_0 A_2)/A} \tag{11}$$

$$\frac{E_{22}}{E_0} = \frac{E_{33}}{E_0} = \frac{1}{1 + c_1[-2\nu_0 A_3 + (1 - \nu_0)A_4 + (1 + \nu_0)A_5 A]/2A} \tag{12}$$

$$\frac{\mu_{12}}{\mu_0} = 1 + \frac{c_1}{\frac{\mu_0}{\mu_1 - \mu_0} + 2c_0 S_{1212}} \tag{13}$$

$$\frac{\mu_{23}}{\mu_0} = 1 + \frac{c_1}{\frac{\mu_0}{\mu_1 - \mu_0} + 2c_0 S_{2323}} \tag{14}$$

$$\frac{\chi_{23}}{\chi_0} = \frac{(1 + \nu_0)(1 - 2\nu_0)}{1 - \nu_0(1 + 2\nu_{12}) + c_1\{2(\nu_{12} - \nu_0)A_3 + [1 - \nu_0(1 + 2\nu_{12})]A_4\}/A} \tag{15}$$

Poisson's ratio is not independent, but can be obtained by

$$\nu_{12}^2 = \frac{E_{11}}{E_{22}} - \frac{E_{11}}{4} \left( \frac{1}{\mu_{23}} + \frac{1}{\chi_{23}} \right) \tag{16}$$

where  $c_1$  and  $c_0$  refer to the volume fractions of voids and matrix, respectively;  $E_{11}$  and  $E_{22}$  (or  $E_{33}$ ) are out-of-plane and in-plane Young's moduli, respectively;  $\mu_{12}$  and  $\mu_{23}$  are in-plane and out-of-plane shear moduli, respectively;  $\chi_{23}$  is a bulk modulus;  $\nu_{12}$  is a Poisson's ratio;  $E_0$ ,  $\mu_0$ ,  $\chi_0$  and  $\nu_0$  are Young's modulus, shear modulus, bulk modulus and Poisson's ratio of the matrix, respectively;  $S_{ijkl}$  is Eshelby's tensor; and the constants ( $A_1, A_2, A_3, A_4, A_5, A$ ) are given in Appendix B.

The coupled relation between equations (15) and (16) can be decoupled by substituting the former into the latter, resulting in the major Poisson's ratio

$$\nu_{12} = \frac{\nu_0 A - c_1(A_3 - \nu_0 A_4)}{A + c_1(A_1 + 2\nu_0 A_2)}. \tag{17}$$

2.3. Two-dimensional randomly oriented voids

When ellipsoidal voids are randomly oriented in the 2–3 plane (refer to Fig. 1 for orientation notation), the porous material also possesses a transverse isotropy. The out-of-plane Young's modulus can be expressed as

$$\frac{E_{11}}{E_0} = \frac{1}{1 + c_1 p_{11}} \tag{18}$$

where

$$p_{11} = \frac{1}{2c_0} \left[ \frac{2\nu_0 S_{2211} + (1 - \nu_0)(S_{1111} - 1)}{2S_{1122}S_{2211} - (S_{1111} - 1)(S_{2222} + S_{2233} - 1)} + \frac{1 + \nu_0}{S_{2233} - S_{2222} + 1} \right]. \quad (19)$$

The out-of-plane shear modulus is

$$\frac{\mu_{12}}{\mu_0} = \frac{\mu_{13}}{\mu_0} = \frac{1}{1 + c_1 p_{21}} \quad (20)$$

where

$$p_{21} = -\frac{1}{2c_0} \left[ \frac{1}{2S_{1313} - 1} + \frac{1}{2S_{2323} - 1} \right]. \quad (21)$$

The isotropic in-plane Young's modulus is

$$\frac{E_{22}}{E_0} = \frac{E_{33}}{E_0} = \frac{1}{1 + c_1 p_{22}} \quad (22)$$

where

$$p_{22} = \frac{1}{c_0} \frac{2(3 - \nu_0)(S_{2222} + S_{2233} - 1) - 2(1 - 7\nu_0)S_{1122} - 2(1 - 3\nu_0)S_{2211} + (3 - 5\nu_0)(S_{1111} - 1)}{16[2S_{1122}S_{2211} - (S_{1111} - 1)(S_{2222} + S_{2233} - 1)]} + \frac{1 + \nu_0}{c_0} \left[ \frac{3}{16(S_{2233} - S_{2222} + 1)} - \frac{1}{4(2S_{1212} - 1)} \right]. \quad (23)$$

The isotropic in-plane shear modulus is

$$\frac{\mu_{23}}{\mu_0} = \frac{1}{1 + c_1 p_{23}} \quad (24)$$

where

$$p_{23} = \frac{1}{2c_0} \left\{ \frac{2(S_{2222} + S_{2233} - 1 + S_{1122} + S_{2211}) + (S_{1111} - 1)}{4[2S_{1122}S_{2211} - (S_{1111} - 1)(S_{2222} + S_{2233} - 1)]} + \frac{1}{4(S_{2233} - S_{2222} + 1)} - \frac{1}{2S_{1212} - 1} \right\}. \quad (25)$$

The out-of-plane Poisson's ratio under the influence of  $\sigma_{11}$  can be written as

$$\frac{\nu_{12}}{\nu_0} = \frac{\nu_{13}}{\nu_0} = \frac{1 + c_1 p_{12}}{1 + c_1 p_{11}} \quad (26)$$

where

$$p_{12} = \frac{1}{4c_0\nu_0} \left\{ \frac{2\nu_0(S_{2222} + S_{2233} - 1 - S_{2211}) + (1 - \nu_0)[2S_{1122} - (S_{1111} - 1)]}{2S_{1122}S_{2211} - (S_{1111} - 1)(S_{2222} + S_{2233} - 1)} + \frac{1 + \nu_0}{S_{2233} - S_{2222} + 1} \right\} \quad (27)$$

The unidirectionally aligned and two-dimensional randomly oriented ellipsoidal void models were presented in this section. In Section 3, these models are employed to predict the effective elastic constants of thermal spray deposits. The unidirectionally aligned voids correspond to inter-lamellar pores and the two-dimensional randomly oriented voids to trans-lamellar cracks.

### 3. RESULTS AND DISCUSSION

#### 3.1. Analytic expressions of elastic constants for thermal spray deposits

The effective elastic constants of AT13 deposits

are calculated by using constitutive equations developed by Zhao *et al.* [17], who described two different spatial distributions of ellipsoidal voids. The trans-lamellar cracks are assumed to be two-dimensional randomly oriented and the inter-lamellar pores are assumed to be unidirectionally aligned (Fig. 2). Both the cracks and pores are transversely isotropic with respect to the spray direction. Special cases of these models were also derived by Zhao *et al.* [17] for penny-shaped and thin crack voids. All three models are considered in this paper to develop the effective five independent elastic constants of thermal spray deposits. Assuming trans-lamellar cracks as two-dimensional randomly oriented voids

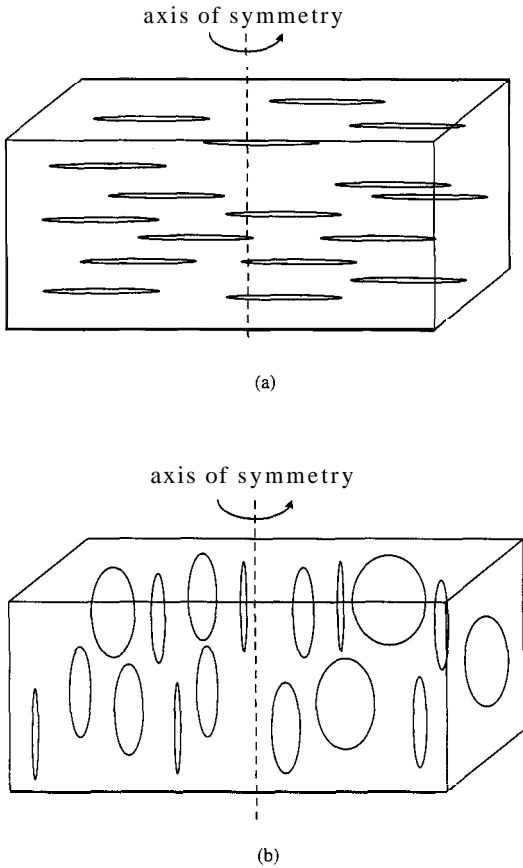


Fig. 2. Spatial distribution of (a) unidirectionally aligned and (b) two-dimensional randomly oriented ellipsoidal voids.

[equations (18)–(24)], and inter-lamellar pores as unidirectionally oriented voids [equations (11)–(17)], the five independent elastic constants are predicted. The spray direction is arbitrarily designated as direction “1” and the other two directions perpendicular to the spray direction are designated as “2” and “3”. These five independent elastic constants provide a complete description of stiffness of the transversely isotropic thermal spray deposits.

The equations of effective elastic constants in Section 2 describe the effective elastic constants in terms of microstructural features. The five independent elastic constants depend on intrinsic (or bulk) elastic constants, the pore volume fraction and the

pore aspect ratio. In other words, the elastic constants normalized by intrinsic elastic constants depend only upon pore volume fraction (or crack density parameter [16]) and pore aspect ratio. The void aspect ratio ( $a$ ) and pore volume fraction (or crack density parameter,  $\eta$ ) are provided by stereological analysis of the void size–shape distribution [22]. This microstructural information is a critical factor which is often approximated when using the theoretical models for elastic constant calculation [26]. It is worth noting that when microstructural information is of interest, a crack density parameter or a pore aspect ratio can be estimated from experimental results of elastic constants.

The superimposition of the unidirectionally and two-dimensional randomly distributed voids models should be carried out to obtain five independent elastic constants of thermal spray deposits. From equation (9) the total strain of the porous material with both unidirectional and two-dimensional randomly distributed voids is estimated to be

$$\epsilon_{kl}^T = \epsilon_{kl}^0 + c_1^{\text{uni}} \epsilon_{kl}^{*,\text{uni}} + c_1^{2\text{D}} \epsilon_{kl}^{*,2\text{D}} \tag{28}$$

where  $c_1^{\text{uni}}$  and  $c_1^{2\text{D}}$  are volume fractions of unidirectionally and two-dimensional randomly distributed voids, respectively; and  $\epsilon_{kl}^{*,\text{uni}}$  and  $\epsilon_{kl}^{*,2\text{D}}$  are the equivalent transformation tensors of unidirectionally and two-dimensional randomly distributed voids, respectively. The effective stiffness tensor of the porous material can be calculated from equations (1)–(10) and (28).

The three different models which describe both unidirectionally and two-dimensional randomly distributed voids are superimposed to estimate the elastic constants of thermal spray deposits. The unidirectionally and two-dimensional randomly distributed models are superimposed with the assumption that porosity is not great enough for the cracks or pores to influence each other.

3.1.1. *Ellipsoidal void model.* The five independent elastic constants of thermal spray deposits estimated from the ellipsoidal void model are given by

$$\frac{E_{11}^T}{E_0} \Big|_{\text{spheroid}} = \frac{1}{1 + c_1^p (A_1 + 2\nu_0 A_2)} \frac{1}{A + c_1^c p_{11}} \tag{29}$$

$$\frac{E_{22}^T}{E_0} \Big|_{\text{spheroid}} = \frac{1}{1 + c_1^p [-2\nu_0 A_3 + (1 - \nu_0) A_4 + (1 + \nu_0) A_5 A]} \frac{1}{2A + c_1^c p_{22}} \tag{30}$$

$$\tag{31}$$

$$\left. \frac{\mu_{23}^T}{\mu_0} \right|_{\text{spheroid}} = 1/1 - \frac{c_1^P}{\frac{\mu_0}{\mu_1 - \mu_0} + 2c_0 S_{2323} + c_1^P} + c_1^c p_{23} \quad (32)$$

$$\left. \frac{\chi_{23}^T}{\chi_0} \right|_{\text{spheroid}} = \frac{(1 + \nu_0)(1 - 2\nu_0)}{c_1^P \{2A_3(\nu_{12}^T - \nu_0) + A_4[1 - \nu_0(1 + 2\nu_{12}^T)]\} / A + (1 + c_1^c \bar{p}_{\gamma_{23}})[1 - \nu_0(1 + 2\nu_{12}^T)]} \quad (33)$$

where the superscript T refers to the superimposed elastic constants;  $c_1^c$  and  $c_1^P$  are volume fractions of trans-lamellar cracks and inter-lamellar pores, respectively; and  $\bar{p}_{\gamma_{23}}$  is (see Appendix B for constants  $a_1, a_2, a_3, a_4, a, b_1, b_2, b_3, b_4$  and  $b_5$ )

$$\begin{aligned} \bar{p}_{\gamma_{23}} = & \left\{ \left[ c_1^c b_4 - \frac{(1 + c_1^c b_1 + c_1^c b_2)(\nu_{12}^T - \nu_0)}{1 - \nu_0(1 + 2\nu_{12}^T)} \right] (-2a_2 + a_4 - a_5 a) \right. \\ & \left. - \left[ \frac{1 + c_1^c b_5}{2} - \frac{c_1^c b_3(\nu_{12}^T - \nu_0)}{1 - \nu_0(1 + 2\nu_{12}^T)} \right] [2(a_1 - a_2 + a_3) + a_4 + a_5 a] \right\} / 2a \\ & \times 2a \{ 2c_1^c b_3 b_4 - (1 + c_1^c b_5)[1 + c_1^c(b_1 + b_2)] \}. \end{aligned} \quad (34)$$

The Poisson's ratio,  $\nu_{12}^T$ , is obtained by the following relation:

$$\left. \frac{\nu_{12}^T}{\nu_0} \right|_{\text{spheroid}} = \frac{\nu_0 - c_1^P(A_3 - \nu_0 A_4) / A + c_1^c \nu_0 p_{12}}{1 + c_1^P(A_1 + 2\nu_0 A_2) / A + c_1^c p_{11}}. \quad (35)$$

*3.1.2. Penny-shaped void model.* The five independent elastic constants of thermal spray deposits from the penny-shaped voids model are given by

$$\left. \frac{E_{11}^T}{E_0} \right|_{\text{penny}} = \frac{1}{1 + \frac{c_1^P}{c_0} \frac{4(1 - \nu_0^2)}{\pi a} + c_1^c p_{11}} \quad (36)$$

$$\left. \frac{E_{22}^T}{E_0} \right|_{\text{penny}} = \left. \frac{E_{33}^T}{E_0} \right|_{\text{penny}} = \frac{1}{1 + \frac{c_1^P}{c_0} + c_1^c p_{22}} \quad (37)$$

$$\left. \frac{\mu_{12}^T}{\mu_0} \right|_{\text{penny}} = \left. \frac{\mu_{13}^T}{\mu_0} \right|_{\text{penny}} = \frac{1}{1 + \frac{4c_1^P(1 - \nu_0^2)}{c_0(2 - \nu_0)\pi a} + c_1^c p_{21}} \quad (38)$$

$$\left. \frac{\mu_{23}^T}{\mu_0} \right|_{\text{penny}} = 1 / \left\{ 1 + \frac{c_1^P}{1 - c_0} \frac{7 - 8\nu_0}{16(1 - \nu_0)} \frac{\pi a - c_1^P}{\pi a} + c_1^c p_{23} \right\} \quad (39)$$

$$\left. \nu_{12}^T \right|_{\text{penny}} = \frac{\nu_0 + \frac{c_1^P}{2c_0} [(1 - \nu_0)(1 + 2\nu_0)] + c_1^c \nu_0 p_{12}}{1 + \frac{c_1^P}{c_0} \frac{4(1 - \nu_0^2)}{\pi a} + c_1^c p_{11}}. \quad (40)$$

*3.1.3. Thin crack model.* The five independent elastic constants of the thin crack model after the superimposition process are given by

$$\left. \frac{E_{11}^T}{E_0} \right|_{\text{crack}} = \frac{1}{1 + \frac{16}{3}(1 - \nu_0^2)\eta^P + \frac{4}{3}\pi a \eta^c} \quad (41)$$

Table 1. Theoretically calculated and experimentally determined Young's moduli and Poisson's ratio

Elastic constants (GPa)	Models			Experimental results			Ref. [30] <sup>a</sup>	
	Thin crack	Penny-shaped voids	Ellipsoidal voids	Knoop	Four-point bending	Flexural resonance	Sample 1	Sample 2
$E_{11}$	53.1	82.1	80.4	53.5	12.3	49.6	116.0	87.4
$E_{22} (= E_{33})$	74.7	92.6	105.8	65.5	—	—	90.5	80.8
$\nu_{12}$	0.100	0.164	0.160	—	—	—	0.278	0.265
$\mu_{12}$	26.4	44.2	40.0	—	—	—	46.2	24.0
$\chi_{23}$	43.5	75.0	43.7	—	—	—	61.1	55.1

<sup>a</sup>Feedstock: Metco 130 (Sulzer Metco, Westbury, NY). Spray equipment: Sulzer-Plasma-Technik A3000S (APS). Sample 1: gun current = 600 A; porosity = 8.8%. Sample 2: gun current = 400 A; porosity = 9.4%. See original reference for fuller details.

$$E_{0 \text{ crack}}^T = \frac{E_{33}^T}{E_0} \Big|_{\text{crack}} = \frac{l}{1 + \frac{4}{3} \pi a \eta^p + \frac{2}{3} \frac{(1 - \nu_0^2)(4 - 3\nu_0)}{(2 - \nu_0)} \eta^c} \quad (42)$$

$$\frac{\mu_{12}^T}{\mu_0} \Big|_{\text{crack}} = \frac{\mu_{13}^T}{\mu_0} \Big|_{\text{crack}} = \frac{1}{1 + \frac{16}{3} \frac{(1 - \nu_0)}{(2 - \nu_0)} \eta^p + \frac{8}{3} \frac{(1 - \nu_0)}{(2 - \nu_0)} \eta^c} \quad (43)$$

$$\frac{\mu_{23}^T}{\mu_0} \Big|_{\text{crack}} = \frac{1}{1 + \frac{4/3 \pi a \eta^p}{1 - 4/3 \pi a \eta^p} + \frac{4}{3} \frac{(1 - \nu_0)(4 - 3\nu_0)}{(2 - \nu_0)} \eta^c} \quad (44)$$

$$\nu_{12}^T \Big|_{\text{crack}} = \nu_{13}^T \Big|_{\text{crack}} = \frac{\nu_0 + \frac{1}{3} (1 + \nu_0) \pi a \eta^c}{1 + \frac{16}{3} (1 - \nu_0^2) \eta^p + \frac{4}{3} \pi a \eta^c} \approx \frac{\nu_0}{1 + \frac{16}{3} (1 - \nu_0^2) \eta^p} \quad (45)$$

where  $c_1^c$  and  $c_1^p$  are volume fractions of trans-lamellar cracks and inter-lamellar pores, respectively; and  $\eta^c$  and  $\eta^p$  are crack density parameters of trans-lamellar cracks and inter-lamellar pores, respectively.

### 3.2. Theoretical and experimental results

The theoretically calculated five independent elastic constants,  $E_{11}^T$ ,  $E_{22}^T (= E_{33}^T)$ ,  $\mu_{12}^T (= \mu_{13}^T)$ ,  $\chi_{23}^T$ , and  $\nu_{12}^T$  are presented in Table 1. The "splat Young's modulus"<sup>†</sup> of AT13 obtained from nanoindentation is 180 GPa [27] and the Poisson's ratio is assumed to be 0.25. The microstructural factors, i.e. the void aspect ratio, crack density parameter and pore volume fraction, obtained from the stereological analysis, are 0.11, 0.602 and 0.95 (0.54 for inter-lamellar pores and 0.41 for trans-lamellar cracks), respectively [22].

Figure 3 shows the variation of elastic constants as a function of void concentration, which is obtained by superimposing unidirectional and two-

dimensional randomly oriented voids of the penny-shaped void model. The  $E_{11}$  value exhibits a significant variation with void concentration, especially in the range of void concentration 0 to 0.2. As the void aspect ratio decreases (i.e. as the void shape becomes sharper) greater variation is observed (Fig. 4). Considering the fact that the porosity of thermal spray deposits ranges from 0 to 15% with low pore aspect ratio, it is expected that the slight

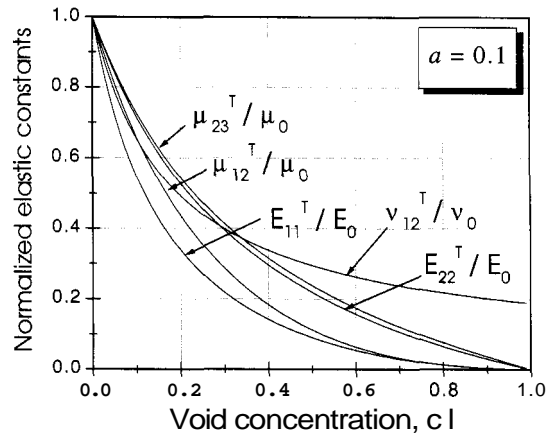


Fig. 3. Elastic constant values as a function of void concentration.

<sup>†</sup>Nanoindentation test was performed within individual splats to determine the near-intrinsic Young's modulus of the deposit, i.e.  $E_0$ . When  $E_0$  is determined,  $\mu_0$  and  $\chi_0$  can be calculated assuming isotropy.

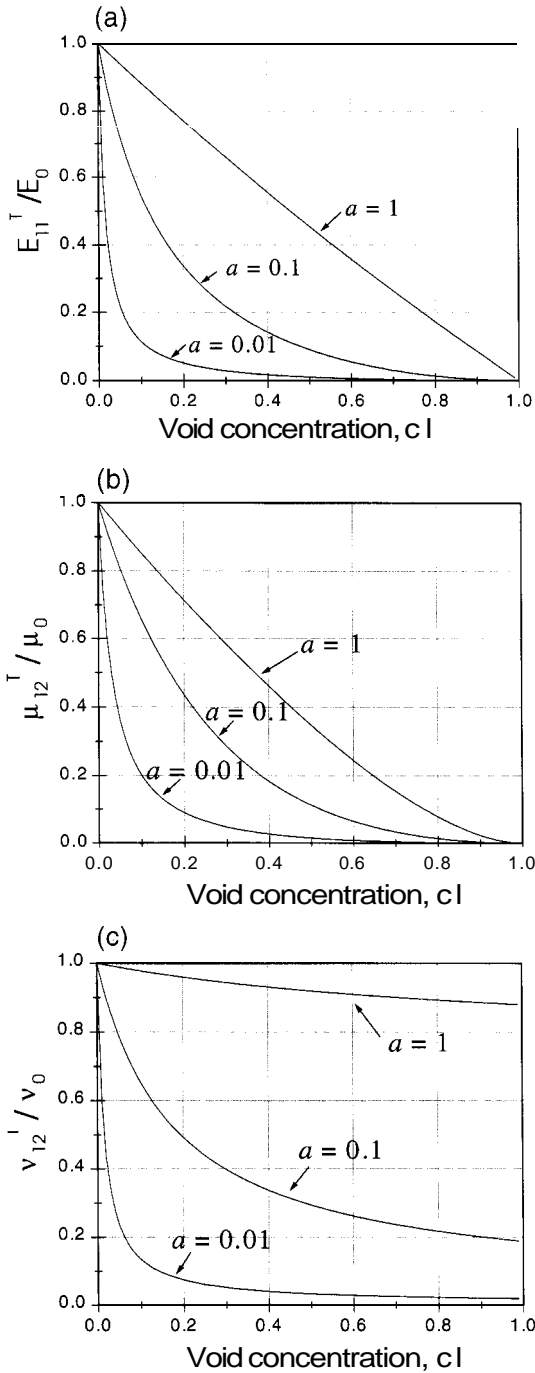


Fig. 4. Variation of (a) Young's modulus, (b) shear modulus, and (c) Poisson's ratio as a function of pore concentration with various void aspect ratios ( $a = 0.01, 0.1, 1$ ).

microstructural changes result in considerable elastic property variations.

The variations of the normalized elastic constants of equations (41)–(45) are plotted with respect to the crack density parameter (Fig. 5). The crack density parameter also has a great influence on the changes in the five independent elastic constants.

The Young's moduli of AT13 exhibit anisotropic behavior. The in-plane Young's modulus,  $E_{22}$  (or

$E_{33}$ ), is greater by a factor of 1.4 than the out-of-plane Young's modulus,  $E_{11}$ . The Young's modulus values determined from various experimental techniques are also given in Table 1. The  $E_{11}$  value from the thin crack model is comparable to the values from flexural resonance and Knoop indentation tests. The experimental value of  $E_{22}$  is about 15% higher than the thin crack model.

The shear moduli are also anisotropic, i.e.  $\mu_{23}$  (33.6 GPa) is 27% higher than  $\mu_{12}$ . The shear modulus measured using the torsional vibration technique was 12.1 GPa. However, this result is a mixture of  $\mu_{12}$  and  $\mu_{23}$  [28]

$$\frac{1}{\mu_{tv}} = \frac{1}{2} (S_{44} + S_{55}) \quad (46)$$

where  $\mu_{tv}$  is the experimental result from a torsional vibration test, and  $S_{44}$  and  $S_{55}$  refer to the elastic compliances which correspond to  $1/\mu_{23}$  and  $1/\mu_{31}$  ( $= 1/\mu_{12}$ ), respectively. Since the ratio of  $\mu_{23}$  and  $\mu_{12}$  can be estimated from the theoretical model ( $\mu_{23}/\mu_{12} = 1.27$ ), the approximate values of  $\mu_{23}$  and  $\mu_{12}$  from torsional experiments are determined to be about 13.7 and 10.1, respectively, which is substantially lower than the theoretical model.

Parthasarathi *et al.* [29] measured a stiffness tensor of  $Al_2O_3$ –13 wt%  $TiO_2$  (Metco 130) thermal-sprayed deposit which included five independent components ( $C_{11}, C_{22}, C_{66}, C_{12}$  and  $C_{23}$ ). These values are converted to practical elastic constants and presented in Table 1. Since spray processes and feedstock powders are different from this paper, a direct comparison is difficult. However, the distinct difference of the results, compared to the results of this paper, is that  $E_{11}$  is greater than  $E_{22}$  and  $\nu_{12}$  is similar to the bulk material.

### 3.3. Poisson's ratio

Although no experimental results of Poisson's ratio of AT13 have been reported, it is worthwhile discussing the Poisson's ratio of thermal spray

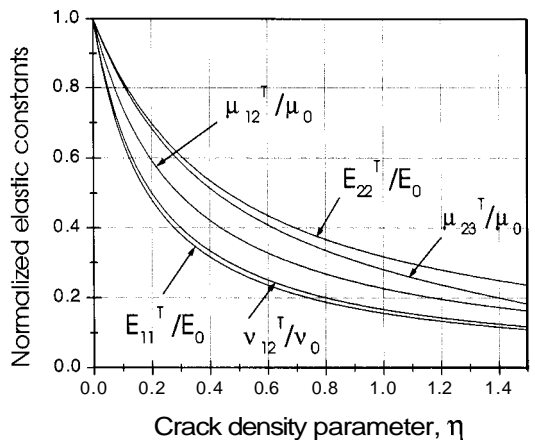


Fig. 5. Variation of normalized elastic constant with crack density parameter.

deposits based on the theoretical results of Section 3.2.

Only a few Poisson's ratio values of thermal spray materials have been reported [2, 29–34]. However, extensive discussion has not been made in the open literature on this subject. One difficulty associated with Poisson's ratio is that it is necessary to accurately measure relatively small strains perpendicular to a uniaxial applied stress direction to obtain reliable Poisson's ratio data. Another important aspect to be carefully considered is the anisotropic nature of the deposits. Transversely isotropic materials require five independent elastic constants, i.e. four elastic constants should be known to determine Poisson's ratio [equation (47)], whereas isotropic materials require only two of Young's, shear or bulk modulus [equation (48)]:

$$\nu_{12} = \sqrt{E_{11} \left( \frac{1}{E_{22}} - \frac{1}{4\mu_{23}} - \frac{1}{4\chi_{23}} \right)} \quad (47)$$

$$\nu = \frac{3\chi - 2\mu}{6\chi + 2\mu}, \quad \nu = \frac{E}{2\mu} - 1 \quad (48)$$

Numerous studies report theoretical and experimental results of effective Poisson's ratio of porous materials [17, 26, 35–37]. It is shown that the effective Poisson's ratio of porous materials may increase, decrease, or remain unchanged as a function of pore concentration depending on the pore shape and the Poisson's ratio of the bulk material [26]. Dominec *et al.* [38] reported a negative effective Poisson's ratio for bismuth–cuprate superconductors. The possibility of a negative Poisson's ratio was confirmed by Dunn and

Ledbetter [26]. However, further study is needed to confirm such values.

Some Poisson's ratio values of thermal spray deposits are given in Table 2. It is noted that some values are greater than intrinsic values, such as 0.304 for Al<sub>2</sub>O<sub>3</sub>–13 wt% TiO<sub>2</sub> [30], and 0.293 for Al<sub>2</sub>O<sub>3</sub>–25 wt% ZrSiO<sub>2</sub> [31]. Unlike other elastic constants, which vary monotonically with porosity [26], the values in Table 2 show that the Poisson's ratio of thermal spray deposits exists over a wide range, i.e. values can increase, decrease or be constant with respect to those of the bulk materials. As shown in Fig. 4(c) (although this theoretical model predicts a monotonic decrease in Poisson's ratio with porosity changes), the Poisson's ratio is substantially sensitive to the porosity and pore shape (i.e. void concentration and void aspect ratio), especially in the range of void concentration 0–0.2. Since the porosity of thermal spray deposits is normally in the 0 to 15% range, it is expected that thermal spray deposits exhibit a wide range of Poisson's ratio, i.e. Poisson's ratio is very sensitive to numerous factors such as the type of spray process, spray conditions, feedstock materials and post treatments.

The effective Poisson's ratio values of thermal spray deposits in different directions are reported by McPherson and Cheang [2] and Parthasarathi *et al.* [29] (Table 2), which indicates that the Poisson's ratio is also anisotropic like other elastic constants. Parthasarathi *et al.* [29] showed that all three values ( $\nu_{12}$ ,  $\nu_{21}$  and  $\nu_{23}$ ) are different, i.e.  $\nu_{12}$  and  $\nu_{21}$  are considerably higher than  $\nu_{23}$ , and  $\nu_{12}$  remains unchanged or slightly higher than that of the bulk material. McPherson and Cheang [2] reported relatively low values and an anisotropic Poisson's ratio.

The Poisson's ratio values are normally shown without any notation on the direction. However,

Table 2. Poisson's ratio values of several thermal spray deposits ( $\nu_{12} = \nu_{13}$ ,  $\nu_{21} = \nu_{31}$ ,  $\nu_{23} = \nu_{32}$ )

Material	Process	Poisson's ratio	Test method	Porosity	Reference
Al <sub>2</sub> O <sub>3</sub>	APS	$\nu_{12} = 0.04\text{--}0.09$ $\nu_{21} = 0.03\text{--}0.06$	Tensile	4%	[2]
Al <sub>2</sub> O <sub>3</sub> –13 wt% TiO <sub>2</sub>	APS	$\nu_{12} = 0.278$ $\nu_{21} = 0.217$ $\nu_{23} = 0.138$	Ultrasonic	8.8%	[29]
Al <sub>2</sub> O <sub>3</sub> –13 wt% TiO <sub>2</sub>	APS	$\nu_{12} = 0.265$ $\nu_{21} = 0.245$ $\nu_{23} = 0.137$	Ultrasonic	9.4%	[29]
Al <sub>2</sub> O <sub>3</sub> –13 wt% TiO <sub>2</sub>	APS	0.304	Three-point bend	18.2%	[30]
Cr <sub>2</sub> O <sub>3</sub> –5 wt% SiO <sub>2</sub> –3 wt% TiO <sub>2</sub>	APS	0.131	Three-point bend	7.5%	[30]
Mo	APS	0.200	Three-point bend	14.9%	[30]
$\alpha$ -Al <sub>2</sub> O <sub>3</sub>	WSP	0.234	Ring	–	[31]
Al <sub>2</sub> O <sub>3</sub> –50% ZrSiO <sub>4</sub>	WSP	0.237	Ring	–	[31]
Al <sub>2</sub> O <sub>3</sub> –25% ZrSiO <sub>4</sub>	WSP	0.293	Ring	–	[31]
Al <sub>2</sub> O <sub>3</sub> –10% ZrSiO <sub>4</sub>	WSP	0.271	Ring	–	[31]
ZrO <sub>2</sub> –7 wt% Y <sub>2</sub> O <sub>3</sub>	APS	0.18	Tensile	3–7%	[32]
WC–12% Co	J-Gun	0.21	Tensile	–	[33]
	APS	0.32	–	–	–
WC–17% Co	HVOF	0.278	Cantilever beam	–	[34]
ZrO <sub>2</sub> –8% Y <sub>2</sub> O <sub>3</sub>	APS	0.181	Cantilever beam	–	[34]
Ni–5% Al	Wire arc	0.163	Cantilever beam	–	[34]
Stainless steel	Wire arc	0.151	Cantilever beam	–	[34]

due to the anisotropic nature, when reporting or consulting any Poisson's ratio of thermal spray deposits, discreet consideration is required on the measurement orientation.

#### 4. CONCLUSIONS

The effective elastic constants of the thermal spray deposits were predicted by using constitutive equations [39]. The quantitative microstructural data obtained from stereological analysis were critical parameters for executing constitutive equations. The models of unidirectionally aligned and two-dimensional randomly distributed voids were employed to estimate the effect of voids on the effective elastic constants of thermal spray deposits. The predicted Young's modulus values from the theoretical calculation were comparable to the obtained experimental values. The theoretical model showed that the effective elastic constants of thermal spray deposits exhibited a large variation with void concentration, crack density parameter and void aspect ratio.

The elastic constants of thermal spray deposits are strongly dependent on microstructures, which are sensitive to the material processing condition. Therefore, the variable elastic constants should be regarded as inherent properties of thermal spray deposits and it is worthwhile to further investigate the explicit relationships of microstructure and numerous microstructural features of thermal spray deposits.

*Acknowledgements*—One of the authors (CCB) thanks NSF-MRSEC DMR-9632570 for partial support.

#### REFERENCES

1. Nakahira, H., Tani, K., Miyajima, K. and Harada, Y., in *Thermal Spray: International Advances in Coatings Technology*, ed. C.C. Berndt. ASM International, Materials Park, OH, 1991, pp. 1011–1017.
2. McPherson, R. and Cheang, P., in *High Performance Ceramic Films and Coatings*, ed. P. Vincenzini. Elsevier, Amsterdam, 1991, pp. 277–290.
3. Wang, D. and Berndt, C.C., in *Proc. 2nd Plasma-Technik-Symposium*, Vol. 2, Ed. S. Blum-Sandmeier, H. Eschnauer, P. Huber and A.R. Nicoll. Lucerne, Switzerland, 1991, pp. 295–304.
4. Coble, R.L. and Kingery, W.D., *J. Am. Ceram. Soc.*, 1956, **39**(11), 377.
5. Knudson, F.P., *J. Am. Ceram. Soc.*, 1959, **42**(8), 376.
6. Hashin, Z., *J. appl. Mech.*, 1962, 00, 143.
7. Rossi, R.C., *J. Am. Ceram. Soc.*, 1968, **51**(8), 433.
8. Dean, E.A., *J. Am. Ceram. Soc.*, 1983, **66**(12), 849.
9. Ashkin, D., Haber, R.A. and Wachtman, J.B., *J. Am. Ceram. Soc.*, 1990, **73**(11), 3376.
10. Ramakrishnan, N. and Arunachalam, V.S., *J. Mater. Sci.*, 1990, 25, 3930.
11. Einstein, A., *Ann. Phys.*, 1906, 19, 289.
12. Einstein, A., *Investigations of the Theory of Brownian Movement*. Dover, New York, 1956.
13. MacKenzie, J.K., *Proc. phys. Soc.*, 1950, **63B**, 2.
14. Mori, T. and Tanaka, K., *Acta Metall.*, 1973, **21**(5), 571.
15. Hashin, Z. and Shtrikman, S., *J. Mech. Phys. Solids*, 1963, 11, 127.
16. Budiansky, B. and O'Connell, R.J., *Int. J. Solids Struct.*, 1976, 12, 81.
17. Zhao, Y.H., Tandon, G.P. and Weng, G.J., *Acta Mech.*, 1989, 76, 105.
18. Zimmerman, R.W., *Mech. Mater.*, 1991, 12, 17.
19. Christensen, R.M., *Proc. R. Soc. A*, 1993, 440, 461.
20. Christensen, R.M., *Mechanics of Composite Materials*. John Wiley, New York, 1979.
21. Leigh, S.H., Montavon, G., Coddet, C., Sampath, S., Herman, H. and Berndt, C.C., in *Advances in Thermal Spray Science and Technology*, ed. C.C. Berndt and S. Sampath. ASM International, Materials Park, OH, 1995, pp. 273–278.
22. Leigh, S.H. and Berndt, C.C., *J. Am. Ceram. Soc.*, 1999, 00, 000.
23. Pasandideh-Frad, M. and Mostagimi, J., in *Thermal Spray Industrial Applications*, ed. C.C. Berndt and S. Sampath. ASM International, Materials Park, OH, 1994, pp. 405–414.
24. Tandon, G.P. and Weng, G.J., *Polymer Comp.*, 1984, 5, 327.
25. Tandon, G.P. and Weng, G.J., *Comp. Sci. Technol.*, 1986, 27, 111.
26. Dunn, M.L. and Ledbetter, H., *J. Mater. Res.*, 1995, **10**(11), 2715.
27. Leigh, S.H. and Berndt, C.C., in *Thermal Spray—Meeting the Challenges of the 21st Century*, ed. C. Coddet. ASM International, Materials Park, OH, 1998, pp. 587–592.
28. Schreiber, E., Anderson, O.L. and Soga, N., *Elastic Constants and Their Measurement*. McGraw-Hill, New York, 1973.
29. Parthasarathi, S., Tittmann, B.R., Sampath, K. and Onesto, E.J., *J. Thermal Spray Technol.*, 1995, **4**(4), 367.
30. Tobe, S., Kodama, S., Misawa, H. and Ishikawa, K., in *Thermal Spray Research and Application*, ed. T.F. Beruecki. ASM International, Materials Park, OH, 1990, pp. 171–177.
31. Lauschmann, H., Moravcova, M., Neufuss, K. and Chraska, P., in *Thermal Spray Industrial Applications*, ed. C.C. Berndt and S. Sampath. ASM International, Materials Park, OH, 1994, pp. 699–701.
32. Steffens, H.-D. and Fischer, U., in *Thermal Spray: Advances in Coatings Technology*, ed. D.L. Houck. ASM International, Materials Park, OH, 1988, pp. 167–173.
33. Morishita, T., Whitfield, R.W., Kuramochi, E. and Tanabe, S., in *Thermal Spray: International Advances in Coatings Technology*, ed. C.C. Berndt. ASM International, Materials Park, OH, 1992, pp. 1001–1004.
34. Rybicki, E.F., Shadley, J.R., Xiong, Y. and Greving, D.J., *J. Thermal Spray Technol.*, 1995, **4**(4), 377.
35. Ledbetter, H. and Fortunko, C., *J. Mater. Res.*, 1995, **10**(6), 1352.
36. Ledbetter, H., Kim, S. and Togano, K., *Physica*, 1991, **185C**, 935.
37. Shindo, Y., Ledbetter, H. and Nozaki, H., *J. Mater. Res.*, 1995, **10**(1), 7.
38. Dominec, J., Vasek, P., Svoboda, P., Plechac, V. and Laermans, C., *Mod. Phys. Lett.*, 1992, **B6**, 1049.
39. Sokolnikoff, I.S., *Mathematical Theory of Elasticity*. McGraw-Hill, New York, 1956.

## APPENDIX A

*Nomenclature*

$\sigma_{i,j}$	Stress tensor
$\varepsilon_{i,j}$	Strain tensor
$C_{ijkl}$	Stiffness tensor
$S_{ijkl}$	Elastic compliance
$e_{ij}$	Displacement component
$E$	Young's modulus
$\mu$	Shear modulus
$\chi, K$	Bulk modulus
$\nu$	Poisson's ratio
$C_{ijkl}^0$	Stiffness tensor of a matrix
$C_{ijkl}^1$	Stiffness tensor of a composite
$\bar{\sigma}_{ij}$	Uniform stress applied to a material
$\varepsilon_{kl}^0$	Strain in a reference material
$\tilde{\sigma}_{ij}$	Deviation from average stress in the matrix due to the inclusion
$\tilde{\varepsilon}_{ij}$	Deviation from average strain in the matrix due to the inclusion
$\sigma_{ij}^{(0)}$	Average stress of the matrix due to the inclusion
$\sigma_{ij}^{pt}$	Perturbed stress
$\varepsilon_{kl}^{pt}$	Perturbed strain
$\sigma_{ij}^{(1)}$	Average stress of the inclusion
$\varepsilon_{kl}^*$	Equivalent transformation strain (tensor)
$S_{ijkl}$	Eshelby's tensor
$c_1$	Volume fraction of inclusion
$c_0$	Volume fraction of matrix
$E_{11}$	Effective out-of-plane Young's modulus
$E_{22}$	Effective in-plane Young's modulus
$\mu_{12}$	Effective in-plane shear modulus
$\mu_{23}$	Effective out-of-plane shear modulus
$\chi_{23}$	Effective bulk modulus
$\nu_{12}$	Effective Poisson's ratio
$E_0$	Young's modulus of the matrix
$\mu_0$	Shear modulus of the matrix
$\chi_0$	Bulk modulus of the matrix
$\nu_0$	Poisson's ratio of the matrix
$a$	Aspect ratio of ellipsoidal inclusion
$\eta$	Crack density parameter
$\varepsilon_{kl}^T$	Superimposed strain of materials with both unidirectionally and two-dimensional randomly distributed voids
$c_1^{\text{uni}} = c_1^{\text{P}}$	Volume fraction of unidirectionally distributed voids (inter-lamellar pores)
$c_1^{2\text{D}} = c_1^{\text{C}}$	Volume fraction of two-dimensional randomly distributed voids (trans-lamellar cracks)
$\varepsilon_{kl}^{*,\text{uni}}$	Equivalent transformation strain of unidirectionally distributed voids
$\varepsilon_{kl}^{*,2\text{D}}$	Equivalent transformation strain of two-dimensional randomly distributed voids
$\eta^{\text{P}}$	Crack density parameter of inter-lamellar pores
$\eta^{\text{C}}$	Crack density parameter of trans-lamellar cracks
$\mu_{\text{tv}}$	Shear modulus results from torsional vibration test
$E_{11}^{\text{T}}$	Superimposed out-of-plane Young's modulus
$E_{22}^{\text{T}}$	Superimposed in-plane Young's modulus
$\mu_{12}^{\text{T}}$	Superimposed in-plane shear modulus
$\mu_{23}^{\text{T}}$	Superimposed out-of-plane shear modulus
$\chi_{23}^{\text{T}}$	Superimposed bulk modulus
$\nu_{12}^{\text{T}}$	Superimposed Poisson's ratio

## APPENDIX B

*Constants for Five Independent Effective Elastic Constants Containing Unidirectionally Aligned Ellipsoidal Voids*

$$\begin{aligned}
 A_1 &= c_0 D (S_{2222} + S_{2233} - 1), \\
 A_2 &= c_0 D S_{1122}, \\
 A_3 &= -c_0 D S_{2211}, \\
 A_4 &= c_0 D (S_{1111} - 1), \\
 A_5 &= [c_0 (S_{2233} - S_{2222} + 1)]^{-1}, \\
 A &= c_0^2 D [2S_{2211} S_{1122} - (S_{1111} - 1)(S_{2222} + S_{2233} - 1)],
 \end{aligned}
 \tag{A1}$$

where

$$D = \frac{(1 + \nu_0)(1 - 2\nu_0)}{\nu_0^2}
 \tag{A2}$$